

# Microscopic dynamical Casimir effect

Reinaldo de Melo e Souza  
*Instituto de Física, Universidade Federal Fluminense,  
CP 24210-346, 24210-346 Niterói, Rio de Janeiro, Brazil*

François Impens and Paulo A. Maia Neto  
*Instituto de Física, Universidade Federal do Rio de Janeiro,  
CP 68528, 21941-909 Rio de Janeiro, Rio de Janeiro, Brazil*  
(Dated: February 26, 2022)

We consider an atom in its ground state undergoing a non-relativistic oscillation in free space. The interaction with the electromagnetic quantum vacuum leads to two effects to leading order in perturbation theory. When the mechanical frequency is larger than the atomic transition frequency, the dominant effect is the motion-induced transition to an excited state with the emission of a photon carrying the excess energy. We compute the angular distribution of emitted photons and the excitation rate. On the other hand, when the mechanical frequency is smaller than the transition frequency, the leading-order effect is the parametric emission of photon pairs, which constitutes the microscopic counterpart of the dynamical Casimir effect. We discuss the properties of the microscopic dynamical Casimir effect and build a connection with the photon production by an oscillating macroscopic metallic mirror.

## I. INTRODUCTION

One of the cornerstones of classical electrodynamics is that accelerated point charges emit radiation. Within the realm of quantum mechanics, one might expect that a ground-state atom undergoing an accelerated motion could also produce radiation. Neutral macroscopic bodies in non-uniform motion are predicted to emit photons out of the quantum vacuum state, an elusive effect that has so far defied experimental verification, and which is known as the dynamical Casimir effect (DCE) (for reviews see [1, 2]). Several geometries [3–8] and material models [9–11] have been analyzed. DCE is greatly enhanced by making use of a cavity resonance [12–19]. Analog models have been proposed [20–24] and realized experimentally [25]. More recently, several applications in quantum information have been investigated [26–29].

Standard treatments of DCE are usually based on boundary conditions (or more generally scattering matrices) for scalar [30–34] or vector field operators [35–37] satisfying the macroscopic Maxwell equations. In this paper, we investigate the microscopic origin of DCE, by considering a ground-state atom undergoing a center-of-mass oscillation. Instead of boundary conditions or scattering matrices, our approach builds on standard quantum optical Hamiltonian treatments for the coupling between an atom in a highly excited external state of an atom trap and the electromagnetic vacuum state. In the same spirit of the Ewald-Oseen microscopic approach [38] to classical electrodynamics, our main purpose is to gain insight into the physics of the DCE at the more fundamental atomic level and identify possible universal features of this effect.

We consider a standard inertial frame in which the atom oscillates. However, our results can be reinterpreted in terms of a co-moving frame. The key point is that the vacuum state of a quantum field is in general not invariant under a transformation to a non-inertial

frame. For instance, in the Unruh effect, the vacuum is seen as a thermal field by an observer with uniform proper acceleration [39, 40] (for a review see [41]).

Moving atoms provide a particularly illuminating example in connection with the Unruh effect, since they behave as local probes of the quantum field. In the specific Unruh’s scenario of uniform proper acceleration, the excitation of an internal state of a point-like detector [42, 43] or atom [44] coupled to a scalar field was analyzed in detail. More recently, the interplay between entanglement and the Unruh effect for a two-atom system has been investigated [45]. Most theoretical works address the specific case of a constant proper acceleration, in which case no radiation is produced [46, 47].

In contrast, a ground-state atom oscillating at a prescribed frequency does produce radiation, as discussed in this paper. By defining a mechanical frequency scale, we are able to develop a physical picture based on the principle of energy conservation and on the analogy with standard nonlinear optical effects. More general motions can be considered by generalizing our formalism to the case in which the motion contains different Fourier components. Considering an harmonic motion also allows us to build a direct comparison with the results for oscillating planar plates [36] and spheres [48], thus providing insight into the microscopic origin of the DCE.

When the external oscillation frequency  $\omega_{\text{cm}}$  is larger than the atomic internal transition frequency, we show that the leading-order effect is the motion-induced transition to an excited internal state, with the emission of a single photon carrying the excess energy. The opposite limit, with  $\omega_{\text{cm}}$  much smaller than the transition frequencies, is more common for real atom traps. In this case, the external motion is quasi-static with respect to the internal degrees of freedom, but not with respect to the electromagnetic field modes with frequencies smaller than  $\omega_{\text{cm}}$ . Therefore, no real internal transition takes place,

but the low-frequency field modes are parametrically excited by the DCE emission of photon pairs.

Here we calculate the DCE angular and frequency spectra for an atom in free space. Atoms in motion in the vicinity of a material surface gives rise to a variety of additional interesting effects, including nonlocal [49, 50], non-additive [51] and geometric [52] phases, decoherence of the internal degrees of freedom [53], corrections to the Casimir-Polder interaction [47, 54] and nonequilibrium forces [55].

This paper is organized as follows. The next section is dedicated to the motion-induced excitation effect involving a one-photon process. In section III we develop the theory of the microscopic DCE and consider in detail the corresponding two-photon emission process. Final remarks are presented in section IV.

## II. MOTION-INDUCED EXCITATION

Our system is composed by a ground-state atom undergoing a prescribed oscillation in an harmonic trap. We consider a regime where the external atomic motion can be treated classically. Our model approximates the case of semiclassical coherent wave-packets in magnetic or optical atom traps [56]. In order to simplify the notation, we consider in this section a two-level atomic model. Details of the derivation are presented in Appendix B for the more general case of a multi-level atom.

To first order in perturbation theory, the atomic external motion might induce a transition to the excited state, accompanied by the emission of a single photon containing the excess energy, as illustrated by Fig. 1a. Such process is the analog of the Stokes Raman effect with the center-of-mass motion playing the role of the pump field. Instead of inelastic Raman scattering, we have photon emission out of the vacuum field state. We show that the corresponding angular distribution is in general anisotropic, and its shape is determined by the ratio between the mechanical frequency and the transition frequency. Other analogies can be proposed. For instance, in the ionization process by monochromatic radiation, the ionized electron is the analog of the emitted photon, while the incident radiation plays the role of the center-of-mass motion.

We model our system by the Hamiltonian  $H = H_A + H_F + H_{\text{int}}$ , where  $H_A$  stands for the internal atomic degrees of freedom,  $H_F$  for the free electromagnetic field and  $H_{\text{int}}$  describes the atom-field interaction. In the dipole approximation, the interaction Hamiltonian assumes the following form

$$H_{\text{int}}(t) = -\mathbf{d} \cdot \left[ \mathbf{E}(\mathbf{r}(t)) + \frac{\mathbf{v}(t)}{c} \times \mathbf{B}(\mathbf{r}(t)) \right], \quad (1)$$

where  $\mathbf{r}(t)$  is the atomic center of mass position and  $\mathbf{v}(t) = d\mathbf{r}(t)/dt$  the associated velocity. The operators in the interaction picture  $\mathbf{E}$  and  $\mathbf{B}$  represent the electric and magnetic field, respectively, whereas  $\mathbf{d}$  denotes the

atomic electric dipole. We assume the motion to be non-relativistic so that  $v(t) \ll c$  at all times. The second term in the right-hand-side of Eq. (1) stands for the Röntgen contribution and is crucial to assure Lorentz covariance to first order in  $v/c$  [57, 58].

Initially, the atom is in the ground state and the electromagnetic field is in the vacuum state. We investigate the population of one-photon states resulting from the atomic motion. We use the notation  $|s, 1_{\mathbf{k}\lambda}\rangle \equiv |s\rangle \otimes |1_{\mathbf{k}\lambda}\rangle$ , where  $s$  represents the internal ground ( $g$ ) or excited ( $e$ ) state, while  $|1_{\mathbf{k}\lambda}\rangle$  is the one-photon field state with wave-vector  $\mathbf{k}$  and polarization  $\lambda$ . The probability for photon emission after a duration  $T$  is given by standard first-order time-dependent perturbation theory:

$$p_{\mathbf{k}\lambda} = \frac{1}{\hbar^2} \left| \int_0^T \langle 1_{\mathbf{k}\lambda}, e | H_{\text{int}}(t) | g, 0 \rangle dt \right|^2. \quad (2)$$

Note that the absence of permanent dipole moment for the ground state implies that the one-photon emission process only occurs by concomitantly exciting the atom.

When computing (2), we take

$$\mathbf{r}(t) = \mathbf{a} \cos(\omega_{\text{cm}} t) \quad (3)$$

in Eq. (1). We also define the maximum external velocity  $v_m = \omega_{\text{cm}} a$ . We consider long interaction times  $T \gg 1/\omega_0$ , where  $\omega_0$  is the atomic transition frequency. This corresponds to a stationary regime in which only resonant processes contribute. Although we describe the external motion as a classical prescribed trajectory, Eq. (3) defines the energy quantum  $\hbar\omega_{\text{cm}}$  as usual in time-dependent perturbation theory with a sinusoidal perturbation Hamiltonian [59]. Thus, the emitted spectrum only contains a single frequency  $\omega_{\mathbf{k}} = c|\mathbf{k}| = \omega_{\text{cm}} - \omega_0$  as illustrated in Figure 1a, provided that  $\omega_{\text{cm}} > \omega_0$ . Since  $\omega_{\mathbf{k}} < \omega_{\text{cm}}$ , the external amplitude  $a$  is much smaller than the relevant field wavelengths:  $\omega_{\mathbf{k}} a/c < v_m/c \ll 1$ , allowing us to expand the electromagnetic fields in Eq. (1) to linear order in  $a$ .

The number of emitted photons is proportional to the duration  $T$  in the stationary regime, enabling the definition of a photon emission rate  $\Gamma_{\text{MIE}}$  describing the motion-induced excitation (MIE). We express our results in terms of the spontaneous emission rate  $\Gamma_0 = |\langle e | \mathbf{d}(0) | g \rangle|^2 \omega_0^3 / (6\pi\hbar c^3)$  of the two-level atom at rest. We first compute the angular distribution of photons, namely the number of photons emitted per unit of solid angle and per unit time (see Appendix A for details):

$$\frac{d\Gamma_{\text{MIE}}}{d\Omega_{\hat{\mathbf{k}}}} = \frac{\Gamma_0 v_m^2}{4c^2} \Theta(\omega_{\text{cm}} - \omega_0) \left( \frac{\omega_{\text{cm}}}{\omega_0} - 1 \right)^3 \times \left[ 2 \left( \frac{\omega_0}{\omega_{\text{cm}}} \right)^2 (\hat{\mathbf{k}} \cdot \hat{\mathbf{a}})^2 + (\hat{\mathbf{k}} \times \hat{\mathbf{a}})^2 \right]. \quad (4)$$

We have introduced the Heaviside function defined as  $\Theta(x) = 1$  if  $x \geq 0$  and  $\Theta(x) = 0$  if  $x < 0$ , as well as the

unit vectors  $\hat{\mathbf{k}}$  and  $\hat{\mathbf{a}}$  along the directions of the photon emission and of the atomic motion respectively.

Eq. (4) shows that the angular distribution receives two separate contributions associated to the projections of the wave-vector parallel or perpendicular to the direction of motion. For  $\omega_{\text{cm}} = \sqrt{2}\omega_0$ , these two projections contribute with equal weights, yielding an isotropic radiation in this case. When  $\omega_{\text{cm}}$  is smaller (larger) than  $\sqrt{2}\omega_0$ , the angular distribution is maximum (minimum) along the direction of motion. The radiation emitted by motion-induced excitation can be highly anisotropic, as illustrated in Figs. 1b and 1c.

We take a mechanical frequency barely higher than the atomic transition frequency in Fig. 1b. In this case, the moving atom radiates nearly twice along the direction of motion as compared to the orthogonal direction. In classical electrodynamics, emission by an accelerated point-like electric dipole along the direction of motion is also possible [60]. However, no classical analogy is available when the frequency scales for the atomic dipole fluctuations ( $\omega_0$ ) and for the external motion ( $\omega_{\text{cm}}$ ) are comparable. On the other hand, when  $\omega_{\text{cm}} \gg \omega_0$ , the distribution illustrated by Figure 1c approaches a classical antenna-like angular distribution. In this limit, the slow dipole fluctuations may be neglected during the fast center of mass oscillation. The resulting radiation pattern may then be constructed by averaging the classical distribution over all possible atomic dipole orientations. This is illustrated by the inset of Fig. 1c, which suggests that the radiation field can be obtained by the superposition of the fields produced by the oscillating point charges with opposite signs.

For a multi-level atom, Eq. (4) gives the contribution of each possible transition to the total angular distribution. Since the atomic excitation is accompanied by the emission of a single photon, we can obtain the excitation rate  $\Gamma_{\text{MIE}}$  for the transition of frequency  $\omega_0$  by integrating the r.h.s. of (4) over the solid angle:

$$\frac{\Gamma_{\text{MIE}}}{\Gamma_0} = \frac{2v_m^2}{3c^2} \Theta(\omega_{\text{cm}} - \omega_0) \left(1 + \frac{\omega_0}{\omega_{\text{cm}}}\right)^2 \left(\frac{\omega_{\text{cm}}}{\omega_0} - 1\right)^3 \quad (5)$$

The excitation rate scales as  $(v_m/c)^2$  [61] and is an increasing function of the center-of-mass frequency  $\omega_{\text{cm}}$ . The frequency dependence results in part from the density of field modes at frequency  $\omega = \omega_{\text{cm}} - \omega_0$  to which the ground-state atom is resonantly coupled through the atomic motion, given that the atom ends up in an excited state (see Fig. 1a). Indeed, the larger the difference between  $\omega_{\text{cm}}$  and the  $\omega_0$ , the larger the density of vacuum modes accessible for the coupling through motion-induced excitation. Should the mechanical frequency be smaller than the transition frequency, no resonant process can take place to first order in the interaction. The corresponding contribution then vanishes, as indicated by the presence of the Heaviside function in (4) and (5). However, photon emission through higher-order resonant processes may still occur in this case, as discussed in the next section.

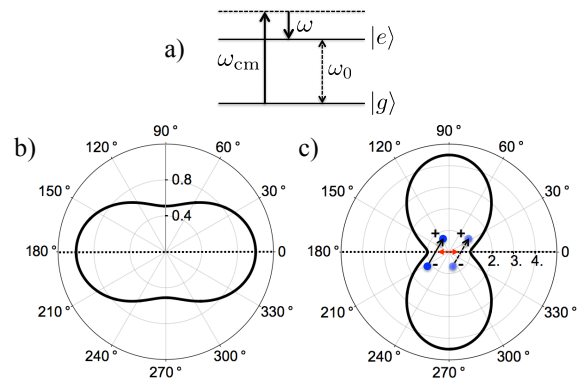


FIG. 1. (a) Energy level diagram for the motion-induced excitation showing the internal ( $\omega_0$ ), external ( $\omega_{\text{cm}}$ ) and photon ( $\omega$ ) frequencies. (b,c) Angular distribution of the light emitted through motion-induced excitation for (b)  $\omega_{\text{cm}} = 1.01\omega_0$  and (c)  $\omega_{\text{cm}} = 3\omega_0$ . The distributions are normalized by the value of the emission rate per unit solid angle along the direction of the external motion, which is indicated by a horizontal dashed line.

### III. MICROSCOPIC DYNAMICAL CASIMIR EFFECT

In this section, we consider the microscopic DCE arising from a ground-state atom undergoing a mechanical oscillation. We assume that the external frequency is smaller than the smallest atomic transition frequency. In this case, and differently from the previous section, only virtual atomic excitations may occur up to second-order in the interaction [62], and the atom stays in the ground state at all times, as illustrated by Fig. 2a. The atom-field interaction may then be described by an effective Hamiltonian obtained from the standard dipolar Hamiltonian through a unitary transformation [63]:

$$H_{\text{eff}}^{\text{rest}}(\mathbf{r}) = -\frac{1}{2} \sum_{\mathbf{k}\lambda} \alpha(\omega_{\mathbf{k}}) \mathbf{E}_{\mathbf{k}\lambda}(\mathbf{r}) \cdot \mathbf{E}(\mathbf{r}), \quad (6)$$

written here for the instantaneous rest frame of the atom. In (6),  $\alpha(\omega)$  stands for the atomic polarizability, given for freely rotating atoms by a sum over all possible excited states [64]

$$\alpha(\omega) = (2/3\hbar) \sum_e \omega_{eg} |e|\mathbf{d}(0)|g\rangle|^2 / (\omega_{eg}^2 - \omega^2). \quad (7)$$

$H_{\text{eff}}^{\text{rest}}$  is quadratic in the electric field and thus leads to the generation of photon pairs out of the vacuum state, as depicted in Fig. 2a and discussed in detail below.

There are two main advantages in using Eq. (6) instead of the more standard dipolar Hamiltonian (1). First, virtual transitions are accounted for through the atomic polarizability so that  $H_{\text{eff}}^{\text{rest}}$  does not operate on the internal atomic degrees of freedom – it simply acts on the Hilbert space associated to the electromagnetic field. Second, the microscopic DCE is obtained already to first order of per-

turbation theory, whereas a more involved second-order derivation would be required when using (1).

In order to obtain a description of the DCE in the laboratory frame, one must Lorentz transform the electric field in Eq. (6). We assume the external motion to be nonrelativistic and expand to first order in  $v/c$ , leading to an effective Hamiltonian in the laboratory frame containing a Röntgen interaction term:

$$H_{\text{eff}} = H_{\text{eff}}^{\text{rest}}(\mathbf{r}(t)) + \frac{\mathbf{v}(t)}{2c} \cdot \sum_{\mathbf{k}\lambda} \alpha(\omega_{\mathbf{k}}) \left[ \mathbf{E}_{\mathbf{k}\lambda}(\mathbf{r}(t)) \times \mathbf{B}(\mathbf{r}(t)) - \mathbf{B}_{\mathbf{k}\lambda}(\mathbf{r}(t)) \times \mathbf{E}(\mathbf{r}(t)) \right], \quad (8)$$

with the field operators taken in the interaction picture.

We consider the sinusoidal motion (3) and the velocity is  $\mathbf{v}(t) = -v_m \sin(\omega_{\text{cm}} t) \hat{\mathbf{a}}$ . The field frequencies are bounded by  $\omega_{\text{cm}}$ , allowing us to expand the rhs of (8) to first order in  $\omega_{\mathbf{k}} a/c \ll 1$  as in Sec. II. However, in contrast with the analysis of Sec. II, we assume that  $\omega_{\mathbf{k}} < \omega_{\text{cm}} \ll \omega_{eg}$ , for all atomic internal transitions so that the relevant field modes are very slow in comparison with the atomic internal dynamics. As a consequence, we see from Eq.(7) that we can approximate the dynamical polarizability by the static one,  $\alpha(\omega_{\mathbf{k}}) \approx \alpha(0) \equiv \alpha_0$ , leading to further simplification of (8). We then find

$$H_{\text{eff}}(t) \approx -\frac{1}{2} \alpha_0 \mathbf{E}^2 + V_\alpha \cos(\omega_{\text{cm}} t) + V_\beta \sin(\omega_{\text{cm}} t) \quad (9)$$

$$V_\alpha = -\frac{1}{2} \alpha_0 \mathbf{a} \cdot \nabla \mathbf{E}^2 \quad (10)$$

$$V_\beta = -\frac{1}{2} \alpha_0 \frac{v_m}{c} \hat{\mathbf{a}} \cdot [\mathbf{E} \times \mathbf{B} - \mathbf{B} \times \mathbf{E}] \quad (11)$$

with all field operators taken at  $\mathbf{r} = \mathbf{0}$ . The production of photon pairs results from the terms which depend explicitly on time, namely the ones proportional to  $V_\alpha$  and  $V_\beta$  in Eq. (9), with the latter accounting for the Röntgen contribution.

It is insightful to build an analogy between  $H_{\text{eff}}$  and the Hamiltonian describing the emission of photon pairs by spontaneous parametric down-conversion in nonlinear crystals [65]. Both Hamiltonians are quadratic in the electric field. Here, the external oscillation plays the role devoted to the laser pump, and the atomic polarizability is the analog of the non-linear susceptibility. The quantum state of the light field resulting from the microscopic DCE can be obtained using first-order time-dependent perturbation theory. Its generic decomposition in terms of two-photon states is given by

$$|\psi(t)\rangle = |0\rangle + \sum_{\mathbf{k}_1 \lambda_1 \mathbf{k}_2 \lambda_2} c_{\mathbf{k}_1 \lambda_1 \mathbf{k}_2 \lambda_2}(t) |1_{\mathbf{k}_1 \lambda_1} 1_{\mathbf{k}_2 \lambda_2}\rangle \quad (12)$$

We compute the two-photon amplitudes  $c_{\mathbf{k}_1 \lambda_1 \mathbf{k}_2 \lambda_2}(t)$  to first order in the perturbation  $H_{\text{eff}}$  and take the rotating-

wave approximation:

$$c_{\mathbf{k}_1 \lambda_1 \mathbf{k}_2 \lambda_2}(t) = -\frac{2\pi \alpha_0 v_m}{L^3 c} (\omega_1 \omega_2)^{1/2} e^{i\Delta\omega t/2} \frac{\sin(\Delta\omega t/2)}{\Delta\omega} \\ \times \hat{\mathbf{a}} \cdot \left[ \frac{c}{\omega_{\text{cm}}} \boldsymbol{\varepsilon}_{\mathbf{k}_1 \lambda_1} \cdot \boldsymbol{\varepsilon}_{\mathbf{k}_2 \lambda_2} (\mathbf{k}_1 + \mathbf{k}_2) \right. \\ \left. + (\hat{\mathbf{k}}_1 \times \boldsymbol{\varepsilon}_{\mathbf{k}_1 \lambda_1}) \times \boldsymbol{\varepsilon}_{\mathbf{k}_2 \lambda_2} + (\hat{\mathbf{k}}_2 \times \boldsymbol{\varepsilon}_{\mathbf{k}_2 \lambda_2}) \times \boldsymbol{\varepsilon}_{\mathbf{k}_1 \lambda_1} \right] \quad (13)$$

where  $\Delta\omega = \omega_1 + \omega_2 - \omega_{\text{cm}}$ . We have introduced the shorthand notation  $\omega_j \equiv \omega_{\mathbf{k}_j}$  and the volume  $L^3$  associated to the quantization of the electromagnetic field.

We now investigate the photon emission spectrum in the stationary regime. By taking the long time limit and squaring the coefficients given by Eq. (13), one retrieves the Fermi golden rule for the probability of two-photon emission. In this limit, energy conservation is enforced and the photon frequencies of the emitted pair satisfy (see Fig. 2a)

$$\omega_1 + \omega_2 = \omega_{\text{cm}}. \quad (14)$$

As a consequence, the frequencies are distributed in the range  $0 \leq \omega \leq \omega_{\text{cm}}$ . The emission probability increases linearly with the interaction time  $t$ , enabling the definition of a stationary radiation emission rate. We first compute the angular spectrum representing the number of photons with polarization  $\lambda$  emitted per unit of time, solid angle and frequency interval. For that purpose, we sum over all possible wavevectors and polarizations for the accompanying photon, as detailed in Appendix B:

$$\frac{d\Gamma_{\text{DCE}}^{(\lambda)}}{d\omega d\Omega_{\hat{\mathbf{k}}}}(\omega, \theta) = \frac{(\alpha_0 v_m)^2}{60\pi^2 c^8} \omega^3 (\omega_{\text{cm}} - \omega)^3 f^{(\lambda)} \left( \frac{\omega}{\omega_{\text{cm}}}, \theta \right) \quad (15)$$

$$f^{(\text{TE})}(x, \theta) = (1-x)^2 (5 \cos^2 \theta + 2) + 5x \quad (16)$$

$$f^{(\text{TM})}(x, \theta) = (1-x)(1-6x) \cos^2 \theta + (1-x)^2 + 5, \quad (17)$$

where  $\theta$  is the angle between the direction of photon emission  $\hat{\mathbf{k}}$  and the direction of motion  $\hat{\mathbf{a}}$ . We have denoted the polarization with the electric field perpendicular to the plane defined by the unit vectors  $\hat{\mathbf{k}}$  and  $\hat{\mathbf{a}}$  as transverse electric (TE), and likewise for the transverse magnetic (TM) one. When  $\theta = 0, \pi$ , the angular spectra must be independent of polarization by symmetry, as can be verified from Eqs. (15)-(17). Our results also check a second symmetry property: the angular spectra must be invariant when replacing  $\theta \rightarrow \pi - \theta$ , since the two opposite directions  $\hat{\mathbf{a}}$  and  $-\hat{\mathbf{a}}$  are equivalent for our harmonic motion when considering long interaction times.

The sign of the coefficient multiplying  $\cos^2 \theta$  in Eqs. (16) and (17) determines the shape of the angular spectrum. For TE polarization, the coefficient  $5(1 - \omega/\omega_{\text{cm}})^2$  is non-negative and hence the distribution is elongated along the direction of motion, except at the upper frequency limit  $\omega \rightarrow \omega_{\text{cm}}$ . At this limit, both

TE and TM distributions become isotropic, but the intensity vanishes as the local density of states becomes arbitrarily small. The TM angular distribution also favors emission close to the direction of motion for frequencies  $\omega < \omega_{\text{cm}}/6$ , but then becomes more elongated perpendicular to this direction for frequencies above  $\omega_{\text{cm}}/6$ , since the coefficient  $(1 - \omega/\omega_{\text{cm}})(1 - 6\omega/\omega_{\text{cm}})$  in (17) becomes negative in this case. Such properties are illustrated by figures 2b and 2c for TE and TM polarizations, respectively.

In short, the direction of motion is always a maximum of the TE distribution and a minimum of the TM one for most of the frequency range. Since the two distributions coincide along this direction, this observation suggests that there are more TM than TE emitted photons. To be more quantitative, we first compute the TE and TM frequency spectra by a solid angle integration of Eq. (15):

$$\frac{d\Gamma_{\text{DCE}}^{(\lambda)}}{d\omega}(\omega) = \frac{(\alpha_0 v_m)^2}{45\pi c^8} \omega^3 (\omega_{\text{cm}} - \omega)^3 F^{(\lambda)}(\omega/\omega_{\text{cm}}) \quad (18)$$

$$F^{(\text{TE})}(x) = 11x^2 - 7x + 11 \quad (19)$$

$$F^{(\text{TM})}(x) = 9x^2 - 13x + 19 \quad (20)$$

in the range  $0 \leq \omega \leq \omega_{\text{cm}}$ . The total frequency spectrum

$$\frac{d\Gamma_{\text{DCE}}}{d\omega}(\omega) = \frac{2(\alpha_0 a)^2}{3\pi c^8} \omega^3 (\omega_{\text{cm}} - \omega)^3 \left[ \omega_{\text{cm}}^2 - \frac{2}{3}\omega(\omega_{\text{cm}} - \omega) \right]$$

is invariant under the transformation  $\omega \rightarrow \omega_{\text{cm}} - \omega$ . This is a direct consequence of the energy conservation condition for the emitted photon pair given by Eq. (14). Indeed, each photon emitted at frequency  $\omega$  is accompanied by a twin emitted at frequency  $\omega_{\text{cm}} - \omega$ . The same property holds for the DCE with a macroscopic planar surface [36]. However, whereas for the latter the TE and TM spectra are also separately symmetric with respect to  $\omega = \omega_{\text{cm}}/2$ , here the TE (TM) spectrum is slightly shifted towards frequencies larger (smaller) than  $\omega_{\text{cm}}/2$ . Such asymmetry arises from the emission of mixed TE-TM pairs, preferably with the TE twin emitted at the upper half of the frequency interval.

We obtain the total emission rates for each polarization by integrating (18) over the frequency interval  $[0, \omega_{\text{cm}}]$ . The resulting TM rate is larger than the TE one by approximately 42%. The total rate is given by  $\Gamma_{\text{atom}} = (23/5670\pi)(\alpha_0 a)^2 \omega_{\text{cm}}^9 / c^8$ . The same frequency dependence can be found in a different context, involving a macroscopic metallic sphere treated in terms of boundary conditions. In fact, we can use the principle of energy conservation in order to derive the total photon emission rate from the result for the vacuum dissipative force on an oscillating perfectly-reflecting sphere obtained in Ref. [48]. When the sphere radius  $R$  is much smaller than the typical field wavelength  $\lambda \sim 2\pi c/\omega_{\text{cm}}$ , we find  $\Gamma_{\text{sphere}} = (1/10368\pi^3)(\alpha_{\text{sph}} a)^2 \omega_{\text{cm}}^9 / c^8$ , where  $\alpha_{\text{sph}} = 4\pi R^3$  is the electric polarizability of the metallic sphere [66].

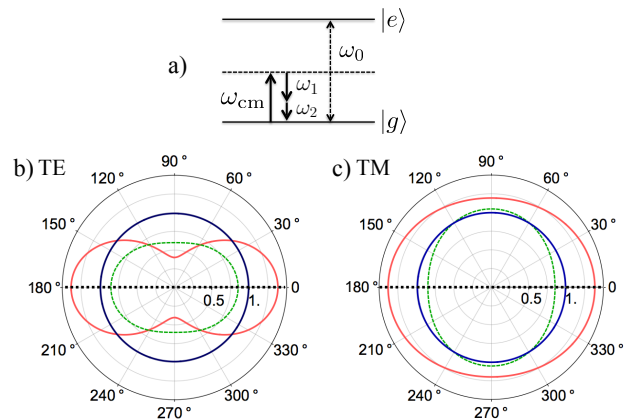


FIG. 2. (a) Energy level diagram for the microscopic dynamical Casimir effect showing the internal ( $\omega_0$ ), external ( $\omega_{\text{cm}}$ ) and photon frequencies ( $\omega_1$  and  $\omega_2$ ). (b,c) DCE angular distributions for (b) TE and (c) TM polarizations. The red (light gray), green (dashed line) and blue (dark gray) correspond to photon frequencies  $\omega = 0.01\omega_{\text{cm}}$ ,  $0.5\omega_{\text{cm}}$  and  $0.99\omega_{\text{cm}}$ , respectively. The distributions are normalized by the value at  $\omega = \omega_{\text{cm}}$  along the direction of the external motion (horizontal dotted line).

Such comparison between the total emission rates for an atom and a metallic sphere suggests that our microscopic approach is capable of explaining several features of the DCE for macroscopic bodies. In classical electrodynamics, physical insight is obtained by treating material media as a collection of dipoles, instead of employing the more standard macroscopic Maxwell equations and the corresponding boundary conditions, as often discussed in the context of the Ewald-Oseen extinction theorem [38].

Here we propose to build the first steps of a similar construction concerning the DCE. In classical electrodynamics, the case of a material medium with a planar interface provides the most illustrative example for the comparison with the microscopic approach. For the DCE, Ref. [36] presents a detailed macroscopic theory of the radiation emitted by an oscillating perfectly-reflecting planar interface. Our results for a single atom already share some common features with the DCE by a planar interface: there are more TM than TE photons, and TE photons are preferably emitted close to the direction of motion. In order to bridge the gap between [36] and our microscopic results, we consider that the material half-space, limited by a planar interface, is constituted of ground-state atoms oscillating in phase along the direction  $\hat{\mathbf{a}}$  perpendicular to the interface. Symmetry of translation parallel to the interface implies that the two photons of a given pair have the same polarization and satisfy the condition

$$\hat{\mathbf{a}} \times (\mathbf{k}_1 + \mathbf{k}_2) = \mathbf{0}, \quad (21)$$

in addition to energy conservation (14). Accordingly, we assume that the emission amplitudes associated to dif-

ferent atoms interfere destructively except for the propagation directions satisfying (21), and for all directions when considering mixed TE-TM pairs.

We now compute the angular spectra from Eq. (13) by enforcing such symmetry conditions. Then, a given  $\mathbf{k}_1$  and  $\lambda_1$  determines a single possibility for the accompanying photon wave-vector  $\mathbf{k}_2$  and polarization  $\lambda_2 = \lambda_1$ . The resulting angular distributions for TE and TM polarizations are sketched in panels (a) and (b) of Fig. 3, respectively. We also show the angular spectra for a perfectly-reflecting plane surface in panels (c) (TE) and (d) (TM) calculated in Ref. [36]. For frequencies in the upper half-interval  $\omega_{\text{cm}}/2 < \omega \leq \omega_{\text{cm}}$ , Eqs. (14) and (21) jointly imply that emission is restricted to the angular sector around the direction of motion given by  $\theta \leq \theta_0 = \arcsin(\omega_{\text{cm}}/\omega - 1)$ . For the atomic case shown in panel (b), the TM distribution develops a sharp peak near the boundary  $\theta_0$ , whereas for the macroscopic perfect reflector shown in panel (d), the TM distribution diverges as  $\theta \rightarrow \theta_0$ . The comparison between the atomic and the perfect reflector distributions indicates that the highly singular behavior of the latter at  $\theta = \theta_0$  results from the unphysical assumption of perfect reflectivity. For all frequencies, the direction of motion is a local minimum for TM photons, and a maximum for TE polarization, in both atomic and macroscopic cases.

Overall, Fig. 3 shows that the main properties of the spectra for a plane perfectly-reflecting surface are already present at the atomic level when considering only photon pairs that do not violate the planar symmetry: TE photons are mostly emitted near the direction of motion, whereas TM photons are preferably emitted as far from this direction as allowed by conditions (14) and (21).

#### IV. CONCLUSION

We have developed a systematic analysis of a ground-state atom undergoing a prescribed non-relativistic motion and coupled to the quantum electromagnetic field, supposed to be initially in the vacuum state. We have assumed an harmonic motion of frequency  $\omega_{\text{cm}}$ . However, more general situations can be obtained from our formalism by Fourier decomposition.

When  $\omega_{\text{cm}}$  is larger than the internal frequency  $\omega_0$ , the external motion drives a transition to an internal excited state, together with the emission of a single photon carrying the excess energy. We have calculated the motion-induced excitation to first order in the perturbation provided by the dipolar Hamiltonian with a Röntgen correction. The photons are emitted according to an angular distribution whose shape depends strongly on the ratio  $\omega_{\text{cm}}/\omega_0$ . The total excitation rate is small since it scales as  $(v_m/c)^2$ . However, it increases with  $\omega_{\text{cm}}/\omega_0$ , with  $\Gamma_{\text{MIE}} \approx (2/3)(v_m/c)^2(\omega_{\text{cm}}/\omega_0)^3\Gamma_0$  for  $\omega_{\text{cm}}/\omega_0 \gg 1$ .

In the opposite case  $\omega_{\text{cm}}/\omega_0 < 1$ , the leading effect is the parametric excitation of photon pairs to second order in the dipolar Hamiltonian. Our approach provides

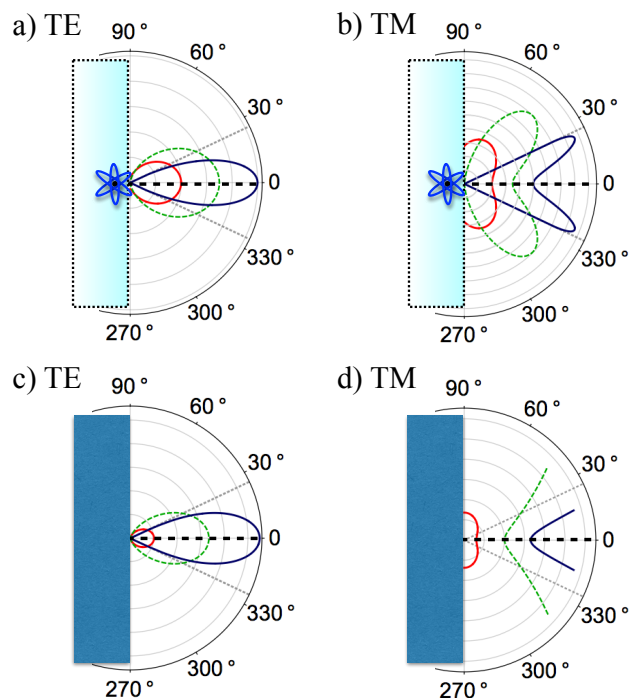


FIG. 3. Comparison between the angular spectra arising from the oscillation of a single atom for (a) TE and (b) TM polarizations, with the spectra for an oscillating perfectly-reflecting mirror, also show for (c) TE and (d) TM polarizations. For the atomic case, we only consider photon pairs satisfying the constraint (21) associated to the planar symmetry. The red (light gray), green (dashed gray) and blue (dark gray) correspond to photon frequencies  $\omega = 0.3\omega_{\text{cm}}$ ,  $0.5\omega_{\text{cm}}$  and  $0.7\omega_{\text{cm}}$ , respectively. In the last case, emission is restricted to the angular sector  $\theta \leq \arcsin(\omega_{\text{cm}}/\omega - 1) \approx 25^\circ$  bounded by the dotted thin lines. Both atom (a,b) and mirror (c,d) oscillate along the direction indicated by the horizontal dashed black line. The angular distributions associated to different frequencies have been plotted using different (arbitrary) scales in (a,b).

a more fundamental perspective into the DCE, which is usually considered for macroscopic bodies with the help of constitutive equations and boundary conditions. We have shown that several properties of the DCE can be explained at the atomic scale. For instance, the dependence of the total emission rate on the oscillation frequency for small compact objects is already obtained within our atomic model.

Another important example is provided by an oscillating plane mirror. We have modelled the material medium as a collection of ground-state atoms. We have assumed destructive interference along the emission directions violating the translational symmetry parallel to the mirror. In this way, we were able to explain the main properties of the emission angular distributions known for perfect metals, although our description is clearly more appropriate for rarefied dielectric materials. This indicates that the DCE for different materials share common universal

features which are already present at the atomic level.

## ACKNOWLEDGMENTS

We thank C. Farina, D. Dalvit, W. Wolff, R. Decca, R. L. Matos, H. Mirandola and G. Bié for valuable discussions and the Brazilian agencies National Council for Scientific and Technological Development (CNPq) and Rio de Janeiro Research Foundation (FAPERJ) for support. P.A.M.N also acknowledges support from the Coordination for the Improvement of Higher Education Personnel (CAPES), the National Institute of Science and Technology Complex Fluids (INCT-FCx), and the São Paulo Research Foundation (FAPESP - 2014/50983-3).

## Appendix A: One-photon process

In this Appendix, we detail the derivations of Sec. II corresponding to the motion-induced excitation. We specify the main steps in order to recover Eq. (4). For clarity, here we write the explicit time dependence of the operators in the interaction picture. We consider the electromagnetic field operators quantized in a finite cubic box of side  $L$ , expressed in Gaussian units as

$$\hat{\mathbf{E}}(r) = \sum_{\mathbf{k}\lambda} i \left( \frac{2\pi\hbar\omega}{L^3} \right)^{1/2} a_{\mathbf{k}\lambda} e^{i\mathbf{k}\cdot\mathbf{r}} \boldsymbol{\varepsilon}_{\mathbf{k}\lambda} + \text{h.c.} \quad (\text{A1})$$

$$\hat{\mathbf{B}}(r) = \sum_{\mathbf{k}\lambda} i \left( \frac{2\pi\hbar\omega}{L^3} \right)^{1/2} a_{\mathbf{k}\lambda} e^{i\mathbf{k}\cdot\mathbf{r}} \hat{\mathbf{k}} \times \boldsymbol{\varepsilon}_{\mathbf{k}\lambda} + \text{h.c.} \quad (\text{A2})$$

h.c. denotes the hermitian conjugate of the series on the right-hand side,  $\omega = |\mathbf{k}|c$ ,  $k \cdot r = \mathbf{k} \cdot \mathbf{r} - \omega t$  and  $\boldsymbol{\varepsilon}_{\mathbf{k}\lambda}$  are the polarization unit vectors. We first evaluate the matrix elements involving the Hamiltonian (1)

$$\begin{aligned} \langle 1_{\mathbf{k}\lambda}, e_s | H_{\text{int}}(t) | g, 0 \rangle &= i \left( \frac{2\pi\hbar\omega}{L^3} \right)^{1/2} \langle e_s | \hat{d}_j(t) | g \rangle \\ &\times e^{-i\mathbf{k}\cdot\mathbf{r}(t)} \left[ (\boldsymbol{\varepsilon}_{\mathbf{k}\lambda})_j + \epsilon_{jmn} \frac{v_m(t)}{c} (\hat{\mathbf{k}} \times \boldsymbol{\varepsilon}_{\mathbf{k}\lambda})_n \right]. \quad (\text{A3}) \end{aligned}$$

We have used Einstein's convention for the summation over repeated indices and introduced the antisymmetric Levi-Civita tensor  $\epsilon_{jmn}$  such that  $\epsilon_{123} = 1$ . We have considered the general case in which there may be several excited states labeled by  $s$ . The coupling (A3) contains simultaneously a static and a velocity-dependent contribution associated respectively to the electric and magnetic components of the Lorentz force. Substituting the above expression into Eq. (2) we obtain for the probability of emission a sum of three terms related to contributions quadratic in the electric field, quadratic in the magnetic field, and bilinear in both fields.

Note that the dipolar matrix elements can be written as  $\langle e_s | \hat{d}_i(t) | g \rangle = \langle e_s | \hat{d}_i(0) | g \rangle e^{-i\omega_s t}$  in the interaction picture, where the frequency  $\omega_s$  corresponds to the Bohr

frequency between the ground state  $g$  and the excited state  $e_s$ . Furthermore, when averaging over the possible atomic dipole configurations, by isotropy one obtains  $\langle e_s | \hat{d}_i(0) | g \rangle \langle g | \hat{d}_j(0) | e_s \rangle = \delta_{ij} |\langle e_s | \mathbf{d}(0) | g \rangle|^2 / 3$ .

From now on, we detail specifically the contribution to the probability of emission  $p_{s\mathbf{k}\lambda}^{(EE)}$  induced by terms quadratic in the electric field. We take the continuum limit  $\sum_{\mathbf{k}} p_{s\mathbf{k}\lambda} \rightarrow \frac{L^3}{8\pi^3} \int d^3\mathbf{k} p_{s\lambda}(\mathbf{k})$  and sum over the possible polarizations  $\lambda$ :

$$p_{s\mathbf{k}}^{(EE)} = \frac{|\langle e_s | \mathbf{d}(0) | g \rangle|^2 \omega}{6\pi^2 \hbar} \int_0^T dt dt' e^{-i(\omega + \omega_s)(t-t')} e^{i\mathbf{k}\cdot(\mathbf{r}(t) - \mathbf{r}(t'))} \quad (\text{A4})$$

As exposed in Sec. II, in the non-relativistic regime one can treat perturbatively the external atomic motion described by Eq. (3), i.e. one expands the complex exponential up to second order in the small parameter  $ka \ll 1$ . It is then convenient to perform a variable change  $(t, t') \rightarrow (\eta = \frac{1}{2}(t + t'), \tau = t - t')$ . Finally, one takes the long time limit, since one monitors the atomic emission over a time which is several orders of magnitude larger than the inverse of the atomic transition frequency. In this stationary limit, only resonant terms contribute to the emission process:

$$p_{s\mathbf{k}}^{(EE)} = \frac{|\langle e_s | \mathbf{d}(0) | g \rangle|^2 \omega T}{12\pi \hbar} (\mathbf{k} \cdot \mathbf{a})^2 \delta(\omega + \omega_s - \omega_{\text{cm}}), \quad (\text{A5})$$

The contributions  $p_{s\mathbf{k}}^{(EM)}$  and  $p_{s\mathbf{k}}^{(MM)}$ , respectively associated to terms bilinear in the electric and magnetic fields and quadratic in the magnetic field, may be obtained by following the same steps. Special care must be taken to work out consistently the perturbative expansion of the complex exponential as to obtain contributions on the order of  $(v/c)^2$ . Finally, by integrating over the frequencies of emission one obtains the angular distribution of emitted photons:  $d\Gamma_{\text{MIE}}/d\Omega_k = (1/T) \sum_s \int_0^\infty (p_{s\mathbf{k}}^{(EE)} + p_{s\mathbf{k}}^{(EM)} + p_{s\mathbf{k}}^{(MM)}) k^2 dk$ . The resulting expression is given by a sum of contributions of the form (4) for each excited state  $e_s$ , with  $\omega_0$  replaced by  $\omega_s$  and  $\Gamma_0$  by the spontaneous emission rate  $\Gamma_s$  between the excited state  $e_s$  and the ground state  $g$ .

## Appendix B: Two-photon process

In this section we present the derivation leading from Eq. (13) to Eq. (15). First of all, from Eq. (12) we see that the probability that two photons are created in the state  $|1_{\mathbf{k}_1\lambda_1} 1_{\mathbf{k}_2\lambda_2}\rangle$  is given in the stationary limit by

$$P_{\mathbf{k}_1\lambda_1, \mathbf{k}_2\lambda_2} = \lim_{t \rightarrow +\infty} |c_{\mathbf{k}_1\lambda_1 \mathbf{k}_2\lambda_2}(t)|^2, \quad (\text{B1})$$

where the limit physically means  $t \gg 1/\Delta\omega$ . Now we use the identity (see for instance [59])

$$\lim_{t \rightarrow +\infty} \frac{\sin^2(\Delta\omega t/2)}{\pi t \Delta\omega^2/2} = \delta(\Delta\omega), \quad (\text{B2})$$

when substituting Eq. (13) into Eq. (B1):

$$\frac{P_{\mathbf{k}_1\lambda_1, \mathbf{k}_2\lambda_2}}{t} = \frac{2\pi^3 \alpha_0^2 \omega_1 \omega_2 v_m^2}{L^6 c^2} \delta(\Delta\omega) \times \left\{ \hat{\mathbf{a}} \cdot \left[ \frac{c}{\omega_{\text{cm}}} (\mathbf{k}_1 + \mathbf{k}_2) (\boldsymbol{\epsilon}_{\mathbf{k}_1\lambda_1} \cdot \boldsymbol{\epsilon}_{\mathbf{k}_2\lambda_2}) + (\hat{\mathbf{k}}_1 \times \boldsymbol{\epsilon}_{\mathbf{k}_1\lambda_1}) \times \boldsymbol{\epsilon}_{\mathbf{k}_2\lambda_2} + (\hat{\mathbf{k}}_2 \times \boldsymbol{\epsilon}_{\mathbf{k}_2\lambda_2}) \times \boldsymbol{\epsilon}_{\mathbf{k}_1\lambda_1} \right] \right\}^2 \quad (\text{B3})$$

The Dirac delta ensures the conservation of energy in the stationary regime. In the continuum limit we have

$$\sum_{\mathbf{k}_1, \mathbf{k}_2} \longrightarrow \frac{L^6}{64\pi^6} \int d^3\mathbf{k}_1 d^3\mathbf{k}_2. \quad (\text{B4})$$

and the probability becomes a density of probability given by

$$\frac{P_{\lambda_1, \lambda_2}(\mathbf{k}_1, \mathbf{k}_2)}{t} = \frac{\alpha_0^2 \omega_1 \omega_2 v_m^2}{32\pi^3 c^2} \delta(\Delta\omega) \times \left\{ \hat{\mathbf{a}} \cdot \left[ \frac{c}{\omega_{\text{cm}}} (\mathbf{k}_1 + \mathbf{k}_2) (\boldsymbol{\epsilon}_{\mathbf{k}_1\lambda_1} \cdot \boldsymbol{\epsilon}_{\mathbf{k}_2\lambda_2}) + (\hat{\mathbf{k}}_1 \times \boldsymbol{\epsilon}_{\mathbf{k}_1\lambda_1}) \times \boldsymbol{\epsilon}_{\mathbf{k}_2\lambda_2} + (\hat{\mathbf{k}}_2 \times \boldsymbol{\epsilon}_{\mathbf{k}_2\lambda_2}) \times \boldsymbol{\epsilon}_{\mathbf{k}_1\lambda_1} \right] \right\}^2 \quad (\text{B5})$$

In order to obtain the photon production rate, we integrate out one of the photons in the pair:

$$P_\lambda(\mathbf{k}) = \sum_{\lambda_2} \int d^3\mathbf{k}_2 P_{\lambda, \lambda_2}(\mathbf{k}, \mathbf{k}_2). \quad (\text{B6})$$

Performing the Fourier space integration in spherical coordinates, we obtain from Eq. (B5)

$$\frac{P_\lambda(\mathbf{k})}{t} = \frac{\alpha_0^2 \omega (\omega_{\text{cm}} - \omega)^3 v_m^2}{32\pi^3 c^5} \sum_{\lambda_2} \int d\Omega_{\mathbf{k}_2} \left\{ \hat{\mathbf{a}} \cdot \left[ \frac{c}{\omega_{\text{cm}}} \left[ \mathbf{k} + \left( \frac{\omega_{\text{cm}}}{c} - k \right) \hat{\mathbf{k}}_2 \right] (\boldsymbol{\epsilon}_{\mathbf{k}_1\lambda_1} \cdot \boldsymbol{\epsilon}_{\mathbf{k}_2\lambda_2}) + (\hat{\mathbf{k}}_1 \times \boldsymbol{\epsilon}_{\mathbf{k}_1\lambda_1}) \times \boldsymbol{\epsilon}_{\mathbf{k}_2\lambda_2} + (\hat{\mathbf{k}}_2 \times \boldsymbol{\epsilon}_{\mathbf{k}_2\lambda_2}) \times \boldsymbol{\epsilon}_{\mathbf{k}_1\lambda_1} \right] \right\}^2 \quad (\text{B7})$$

The angular integrals can be readily evaluated from symmetry considerations by relating them with averages over all spatial directions. Let us then analyze each type of integral required for the evaluation of Eq. (B7). Firstly,

$$\sum_{\lambda_2} \int d\Omega_{\mathbf{k}_2} (\boldsymbol{\epsilon}_{\mathbf{k}\lambda} \cdot \boldsymbol{\epsilon}_{\mathbf{k}_2\lambda_2})^2 = 4\pi \boldsymbol{\epsilon}_i^{\mathbf{k}\lambda} \boldsymbol{\epsilon}_j^{\mathbf{k}\lambda} \sum_{\lambda_2} \overline{\boldsymbol{\epsilon}_i^{\mathbf{k}_2\lambda_2} \boldsymbol{\epsilon}_j^{\mathbf{k}_2\lambda_2}}, \quad (\text{B8})$$

where we employed Einstein summation convention. From symmetry, the tensor obtained by averaging over all directions in the r.h.s. of Eq. (B8) must be isotropic since we have summed over polarizations [67]:

$$\sum_{\lambda_2} \overline{\boldsymbol{\epsilon}_i^{\mathbf{k}_2\lambda_2} \boldsymbol{\epsilon}_j^{\mathbf{k}_2\lambda_2}} = C \delta_{ij} = \frac{2}{3} \delta_{ij}, \quad (\text{B9})$$

where the constant  $C$  were determined by contracting the indexes  $i$  and  $j$  on both sides of the equation. Then, there is a term proportional to  $\sum_{\lambda_2} \overline{\hat{\mathbf{k}}_{2i} \boldsymbol{\epsilon}_j^{\mathbf{k}_2\lambda_2} \boldsymbol{\epsilon}_m^{\mathbf{k}_2\lambda_2}}$  which must be proportional to the only isotropic tensor of rank 3,  $\epsilon_{ijm}$ . However, the latter is antisymmetric in the exchange  $j \leftrightarrow m$ , while the former is symmetric, hence this term must vanish. There are also terms proportional to  $\sum_{\lambda_2} \overline{k_{2i} \boldsymbol{\epsilon}_j^{\mathbf{k}_2\lambda_2}}$ . These must be proportional to  $\delta_{ij}$  and then vanish upon contraction of the indexes. The most difficult integral we must deal with is proportional to

$$\sum_{\lambda_2} \overline{k_{2m} k_{2n} \boldsymbol{\epsilon}_i^{\mathbf{k}_2\lambda_2} \boldsymbol{\epsilon}_j^{\mathbf{k}_2\lambda_2}} = C_1 \delta_{ij} \delta_{mn} + C_2 (\delta_{im} \delta_{jn} + \delta_{in} \delta_{jm}), \quad (\text{B10})$$

where we used the most general form of a 4-rank isotropic tensor symmetric upon the change  $i \leftrightarrow j$ . Imposing that a contraction of  $i$  with  $m$  vanishes while a contraction of  $n$  with  $m$  yields  $2\delta_{ij}/3$ , we obtain the system of equations

$$\begin{aligned} C_1 + 4C_2 &= 0 \\ 3C_1 + 2C_2 &= \frac{2}{3}, \end{aligned} \quad (\text{B11})$$

which yields  $C_1 = 4/15$  and  $C_2 = -1/15$ .

We may evaluate (B7) with the results obtained in the previous paragraphs. In order to obtain Eq. (15), we must only relate the probability of creating a photon with the number of photons created, which is given by the relation

$$d\mathcal{N}_\lambda(\mathbf{k}) = P_\lambda(\mathbf{k}) d^3\mathbf{k} = \frac{P_\lambda(\mathbf{k}) \omega^2}{c^3} d\omega d\Omega_{\hat{\mathbf{k}}} \quad (\text{B12})$$

Defining the rate of photon production by  $\Gamma = \mathcal{N}/t$ , we write the spectral rate of photon creation by solid angle as

$$\frac{d\Gamma_\lambda}{d\omega d\Omega_{\hat{\mathbf{k}}}}(\omega, \hat{\mathbf{k}}) = \frac{\omega^2 P_\lambda(\omega, \hat{\mathbf{k}})}{tc^3}. \quad (\text{B13})$$

[1] V. V. Dodonov, Current status of the dynamical Casimir effect, Phys. Scr. **82**, 038105 (2010).

[2] D. A. R. Dalvit, P. A. Maia Neto and F. D. Mazzitelli,

- Fluctuations, dissipation and the dynamical Casimir effect, *Lect. Notes Phys.* **834**, 287 (2011).
- [3] G. Barton, The quantum radiation from mirrors moving sideways, *Ann. Phys. (N.Y.)* **245**, 361 (1996).
- [4] D. F. Mundarain and P. A. Maia Neto, Quantum radiation in a plane cavity with moving mirrors, *Phys. Rev. A* **57**, 1379 (1998).
- [5] M. Kardar and R. Golestanian, The “friction” of vacuum, and other fluctuation-induced forces, *Rev. Mod. Phys.* **71**, 1233 (1999).
- [6] P. A. Maia Neto, The dynamical Casimir effect with cylindrical waveguides, *J. Opt. B: Quantum Semiclass. Opt.* **7**, S86 (2005).
- [7] , M. Crocce, D. A. R. Dalvit, F. C. Lombardo and F. D. Mazzitelli, Hertz potentials approach to the dynamical Casimir effect in cylindrical cavities of arbitrary section, *J. Opt. B: Quantum Semiclass. Opt.* **7**, S32 (2005).
- [8] A. Manjavacas and F. J. García de Abajo, Vacuum Friction in Rotating Particles, *Phys. Rev. Lett.* **105**, 113601 (2010).
- [9] G. Barton and A. Calogeracos, On the quantum electrodynamics of a dispersive mirror. 1: Mass shifts, radiation, and radiative reaction, *Ann. Phys. (N.Y.)* **238**, 227 (1995).
- [10] R. Gütig and C. Eberlein, Quantum radiation from moving dielectrics in two, three and more spatial dimensions, *J. Phys. A: Math. Gen.* **31**, 6819 (1998).
- [11] J. Sarabadani and M. Miri, Motion-induced radiation in a cavity with conducting and permeable plates, *Phys. Rev. A* **75**, 055802 (2007).
- [12] G. T. Moore, Quantum theory of electromagnetic field in a variable-length one-dimensional cavity. *J. Math. Phys.* **11**, 2679 (1970).
- [13] M. Castagnino and R. Ferraro, The radiation from moving mirrors: The creation and absorption of particles, *Ann. Phys. (NY)* **154**, 1 (1984).
- [14] V. V. Dodonov, A. B. Klimov, and V. I. Man’ko, Generation of squeezed states in a resonator with a moving wall, *Phys. Lett. A* **149**, 225 (1990).
- [15] M.-T. Jaekel and S. Reynaud, Motional Casimir force, *J. Phys. I (France)* **2**, 149 (1992).
- [16] A. Lambrecht, M.-T. Jaekel, and S. Reynaud, Motion induced radiation from a vibrating cavity, *Phys. Rev. Lett.* **77**, 615 (1996).
- [17] D. A. R. Dalvit, and F. D. Mazzitelli, Renormalization-group approach to the dynamical Casimir effect, *Phys. Rev. A* **57**, 2113 (1998).
- [18] G. Schaller, R. Schützhold, G. Plunien and G. Soff, Dynamical Casimir effect in a leaky cavity at finite temperature, *Phys. Rev. A* **66**, 023812 (2002).
- [19] V. Macrì, A. Ridolfo, O. Di Stefano, A. F. Kockum, F. Nori and S. Savasta, Non-perturbative dynamical Casimir effect in optomechanical systems: vacuum Casimir-Rabi splittings, *Phys. Rev. X* **8**, 011301 (2018).
- [20] E. Yablonovitch, Accelerating reference frames for electromagnetic waves in a rapidly growing plasma: Unruh-Davies-Fulling-De Witt radiation and the nonadiabatic Casimir effect, *Phys. Rev. Lett.* **62**, 1742 (1989).
- [21] C. Braggio et al., A novel experimental approach for the detection of the dynamical Casimir effect, *Europhys. Lett.* **70**, 754 (2005).
- [22] J. R. Johansson, G. Johansson, C. M. Wilson, and F. Nori, Dynamical Casimir Effect in a Superconducting Coplanar Waveguide, *Phys. Rev. Lett.* **103**, 147003 (2009).
- [23] F. C. Lombardo, F. D. Mazzitelli, A. Soba and P. I. Villar, Dynamical Casimir effect in superconducting circuits: A numerical approach, *Phys. Rev. A* **93**, 032501 (2016).
- [24] J. Marino, A. Recati and I. Carusotto, Casimir forces and quantum friction from Ginzburg radiation in atomic Bose-Einstein condensates, *Phys. Rev. Lett.* **118**, 045301 (2017).
- [25] C. M. Wilson et al. Observation of the dynamical Casimir effect in a superconducting circuit, *Nature* **479**, 376 (2011).
- [26] C. Sabin and G. Adesso, Generation of quantum steering and interferometric power in the dynamical Casimir effect, *Phys. Rev. A* **92** 042107 (2015).
- [27] C. Sabin, I. Fuentes and G. Johansson, Quantum discord in the dynamical Casimir effect, *Phys. Rev. A* **92**, 012314 (2015).
- [28] R. Stassi, S. De Liberato, L. Garziano, B. Spagnolo and S. Savasta, Quantum control and long-range quantum correlations in dynamical Casimir arrays, *Phys. Rev. A* **92**, 013830 (2015).
- [29] S. Felicetti, M. Sanz, L. Lamata, G. Romero, G. Johansson, P. Delsing and E. Solano, Dynamical Casimir effect entangles artificial atoms, *Phys. Rev. Lett.* **113**, 093602 (2014).
- [30] S. A. Fulling and P. C. W. Davies, Radiation from a moving mirror in two dimensional space-time - conformal anomaly. *Proc. R. Soc. A* **348**, 393-414 (1976).
- [31] L. H. Ford and A. Vilenkin, Quantum radiation by moving mirrors. *Phys. Rev. D* **25**, 2569-2575 (1982).
- [32] M.-T. Jaekel and S. Reynaud, Fluctuations and dissipation for a mirror in vacuum, *Quantum Opt.* **4**, 39 (1992).
- [33] D. T. Alves, C. Farina, and P. A. Maia Neto, Dynamical Casimir effect with Dirichlet and Neumann boundary conditions, *J. Phys. A: Math. Gen.* **36**, 11333 (2003).
- [34] A. L. C. Rego, B. W. Mintz, C. Farina and D. T. Alves, Inhibition of the dynamical Casimir effect with Robin boundary conditions, *Phys. Rev. D* **87** 045024 (2013).
- [35] P. A. Maia Neto, Vacuum radiation pressure on moving mirrors, *J. Phys. A: Math. Gen.* **27**, 2167 (1994).
- [36] P. A. Maia Neto and L. A. S. Machado, Quantum radiation generated by a moving mirror in free space, *Phys. Rev. A* **54**, 3420 (1996).
- [37] M. F. Maghrebí, R. Golestanian, and M. Kardar, Scattering approach to the dynamical Casimir effect, *Phys. Rev. D* **87**, 025016 (2013).
- [38] H. Fearn, D. F. V. James and P. W. Milonni, Microscopic approach to reflection, transmission, and the Ewald-Oseen extinction theorem, *Am. J. Phys.* **64**, 986 (1996).
- [39] P. C. W. Davis, Scalar production in Schwarzschild and Rindler metrics, *J. Phys. A* **8**, 609 (1975).
- [40] W. G. Unruh, Notes on black-hole evaporation, *Phys. Rev. D* **14**, 870 (1976).
- [41] L. C. B. Crispino, A. Higuchi, G. E. A. Matsas, The Unruh effect and its applications, *Rev. Modern Phys.* **80**, 787 (2008).
- [42] W. G. Unruh and R. M. Wald, What happens when an accelerating observer detects a Rindler particle, *Phys. Rev. D* **29**, 1047 (1984).
- [43] V. L. Ginzburg and V. P. Frolov, Vacuum in a homogeneous gravitational field and excitation of a uniformly accelerated detector, *Sov. Phys. Usp.* **30**, 1073 (1987).
- [44] J. Audretsch and R. Müller, Spontaneous excitation of an

- accelerated atom: The contributions of the vacuum fluctuations and radiation reaction, *Phys. Rev. A* **50**, 1755 (1994).
- [45] G. Menezes and N. F. Svaiter, Radiative processes of uniformly accelerated entangled atoms, *Phys. Rev. A* **93**, 052517 (2016).
- [46] D. J. Raine, D. W. Sciama, P. G. Grove, Does a uniformly accelerated quantum oscillator radiate?, *Proc. R. Soc. Lond. A* **435**, 205 (1991).
- [47] B. L. Hu, A. Roura, and S. Shresta, Vacuum fluctuations and moving atom/detectors: from the Casimir-Polder to the Unruh-Davies-DeWitt-Fulling effect, *J. Opt. B: Quantum Semiclass. Opt.* **6**, S698 (2004) and references therein.
- [48] P. A. Maia Neto and S. Reynaud, Dissipative force on a sphere moving in vacuum, *Phys. Rev. A* **47**, 1639 (1993).
- [49] F. Impens, R. O. Behunin, C. C. Ttira, and P. A. Maia Neto, Non-local double-path Casimir phase in atom interferometers, *EPL* **101**, 60006 (2013).
- [50] F. Impens, C. C. Ttira, R. O. Behunin, and P. A. Maia Neto, Dynamical local and nonlocal Casimir atomic phases, *Phys. Rev. A* **89** 022516 (2014).
- [51] F. Impens, C. C. Ttira, and P. A. Maia Neto, Non-additive dynamical Casimir atomic phases, *J. Phys. B: At. Mol. Opt. Phys.* **46**, 245503 (2013).
- [52] F. C. Lombardo and P. Villar, Geometric phase corrections on a moving particle in front of a dielectric mirror, *Europhys. Lett.* **118**, 50003 (2017).
- [53] M. B. Farias and F. C. Lombardo, Dissipation and decoherence effects on a moving particle in front of a dielectric plate, *Phys. Rev. D* **93**, 065035 (2016).
- [54] S. Scheel and S. Buhmann, Casimir-Polder forces on moving atoms, *Phys. Rev. A* **80**, 042902 (2009).
- [55] R. O. Behunin and B.-L. Hu, Nonequilibrium forces between atoms and dielectrics mediated by a quantum field, *Phys. Rev. A* **84**, 012902 (2011).
- [56] Such approach is legitimate if the shape of the atomic wave-function in momentum space is almost unaffected by the atomic recoil, and if the energy stored in the external motion is much larger than the energy quantum of the trap. These conditions can be simultaneously met by considering, for instance, the atomic center of mass to be in a coherent state  $|\alpha\rangle$  with amplitude  $|\alpha| \gg 1$ .
- [57] M. Wilkens, Significance of Röntgen current in quantum optics: Spontaneous emission of moving atoms, *Phys. Rev. A* **49**, 570 (1994).
- [58] C. Baxter, M. Babiker and R. Loudon, Canonical approach to photon pressure, *Phys. Rev. A* **47**, 1278 (1993).
- [59] L. D. Landau and E. M. Lifshitz, *Quantum Mechanics (Course of theoretical physics vol. 3)* (Elsevier, Oxford, 1977), sec. 42.
- [60] J.A. Heras, Radiation fields of a dipole in arbitrary motion, *Am. J. Phys.* **62**, 1109 (1994).
- [61] In order to compute the emission rate to order  $(v/c)^2$ , it is sufficient to expand the interaction Hamiltonian to order  $v/c$  as in (1).
- [62] Up to order  $(v/c)^2$  all processes involve the absorption of a single quantum of vibration  $\hbar\omega_{\text{cm}}$  associated to the atomic center-of-mass. In second order of perturbation theory we have two-photon processes and by energy conservation we have in the stationary regime  $\omega_{\text{em}} = \omega_{0s} + \omega_1 + \omega_2$ , where  $\omega_{0s}$  is the atomic transition frequency to state  $|s\rangle$  and  $\omega_1, \omega_2$  are the frequencies of the produced photons. This can be immediately generalized for any order of perturbation theory and thus we conclude that up to order  $(v/c)^2$  motion-induced excitation only happens if  $\omega_{\text{em}} > \omega_{0s}$  for some state  $|s\rangle$  different from the ground state.
- [63] R. Passante, E. A. Power and T. Thirunamachandran, Radiation-molecule coupling using dynamic polarizabilities: application to many-body forces, *Phys. Lett. A* **249**, 77 (1998).
- [64] D. P. Craig and T. Thirunamachandran, *Molecular quantum electrodynamics* (Academic Press, 1984), page 159.
- [65] M. H. Rubin, D. N. Klyshko, Y. H. Shih, and A. V. Sergienko, Theory of two-photon entanglement in type-II optical parametric down-conversion, *Phys. Rev. A* **50**, 5122 (1994).
- [66] Note that the results for the sphere and the atom are not expected to coincide, since the magnetic dipole moment of a small metallic sphere at rest is comparable with its electric dipole moment.
- [67] An isotropic tensor has the same components in all rotated coordinate systems. The Kronecker  $\delta_{ij}$  is the only isotropic tensor with rank 2, while the Levi-Civita tensor  $\epsilon_{ijk}$  is the only isotropic one with rank 3. From these two tensors we build all other isotropic tensors of different ranks. For more details see G. Temple, *Cartesian tensors: An introduction* (Dover, Mineola, 2004).